Graphene oxide-supported zinc cobalt oxides as effective cathode catalysts for microbial fuel cell: High catalytic activity and inhibition of biofilm formation

Wei Yang,[a,b,c] Gustavo Chata,[c] Yudong Zhang [a,b], Yi Peng,[c] Jia En Lu,[c] Nan Wang,[d] Rene Mercado,[c] Jun Li, [a,b,*] and Shaowei Chen[c,d,*]

[a] Key Laboratory of Low-grade Energy Utilization Technologies and Systems (Chongqing University), Ministry of Education, Chongqing 400030, China. E-mail: lijun@cqu.edu.cn

[b] Institute of Engineering Thermophysics, School of Energy and Power Engineering, Chongqing University, Chongqing 400030, China

[c] Department of Chemistry and Biochemistry, University of California, 1156 High Street, Santa Cruz, California 95064, USA. E-mail: shaowei@ucsc.edu

[d] New Energy Research Institute, School of Environment and Energy, South China University of Technology, Guangzhou Higher Education Mega Center, Guangzhou 510006, China

Abstract

Microbial fuel cell (MFC) is a unique energy technology that can treat wastewater and concurrently generate electricity. However, the MFC performance is typically rather limited due to the sluggish kinetics of oxygen reduction reaction (ORR) and insufficient ion transfer on the cathode. Thus, development of high-performance ORR catalysts with enhanced ion transfer is of fundamental significance for the wide-spread application of MFC. In this study, nanocomposites (GO-Zn/Co) based on graphene oxide-supported cobalt and zinc oxide nanoparticles were synthesized by a hydrothermal treatment of graphene oxide and cobalt and zinc acetates followed by pyrolysis at controlled temperatures. The porosity of the resulting nanocomposites was found to vary with the pyrolysis temperature and Zn/Co mole ratios. The sample prepared at 800 °C with a Zn/Co mole ratio of 1:1 exhibited the best ORR performance in alkaline media among the series, with a high halfwave potential of +0.81 V vs. RHE. Notably, the resultant GO-Zn/Co nanocomposites exhibited an apparent antibacterial activity, inhibiting the formation of biofilms on the cathode surface. An MFC using the as-prepared GO-Zn/Co as the cathode catalyst achieved a maximum power density (773 mW m^{-2}) that was even higher than that with state-of-art Pt/C catalyst (744 mW m^{-2}), and the power output remained virtually unchanged during continuous operation for one month. The results suggest that the GO-Zn/Co nanocomposites can serve as a viable alternative for MFC cathode catalysts.

Keywords: microbial fuel cell, oxygen reduction reaction, ion diffusion, antibacterial, biofilm

1. Introduction

The environmental issues associated with the consumption of fossil fuels have stimulated the development of renewable energy technologies, such as microbial fuel cell (MFC). MFC generates electricity through the metabolism of organic compounds, whereby power production and wastewater treatment occur in a sustainable fashion by select bacteria (e.g., *Shewanella* and *Geobacter*) [1-3]. Therefore, MFC has been attracting extensive attention in recent years. Although substantial progress has been achieved, the relatively low power density has markedly hindered their commercial applications, as compared to other energy conversion technologies [4]. Among the various forms of MFC, air-cathode MFC has been considered as a sustainable design, due to the ready availability of oxygen from air [5, 6].

The performance of an air-cathode MFC is affected by a number of factors, such as the oxidation rate of the substrate molecules, electron transfer between bacteria and anode, ORR kinetics on cathode, and ohmic/mass transport losses [7-12]. Among these, ORR kinetics on the cathode is a dominating factor that largely dictates the overall MFC performance. Platinum-based nanoparticles have been used extensively as the catalysts of choice towards ORR, but the applications have been severely limited due to their high costs and unsatisfactory durability under relevant MFC conditions [13-15]. Within this context, materials derived from non-noble metal precursors have been widely used as active components for ORR electrocatalysis, due to their high natural abundance, low costs, and apparent electrocatalytic activity [15-20]. Among these, spinel-type cobalt oxide (Co_3O_4) has been attracting particular attention as ORR catalysts [21, 22]. Notably, Co-based spinel bimetallic structure such as $ZnCo_2O_4$ are of unique interest, primarily because Zn^{2+} in $ZnCo_2O_4$ can replace non-active Co^{2+} at the tetrahedral sites and provide an enhanced utilization of the highly active Co^{3+} species at the octahedral sites [23-26]. Yet, despite an apparent catalytic activity, the application of $ZnCo_2O_4$ in ORR electrocatalysis has remained challenging due to its unsatisfactory stability and conductivity [27].

To mitigate these issues, an effective approach is to prepare composites of $ZnCo_2O_4$ with graphene, by taking advantage of the excellent conductivity, high theoretical surface area and remarkable stability of the carbon scaffolds [28, 29]. Also, with the incorporation of nitrogen dopants, the ORR activity of the carbon-supported $ZnCo_2O_4$ nanocomposites can be further enhanced due to the formation of functional moieties, such as pyridinic-N, graphitic-N, and Co-N species, that are known to be ORR active [30-32]. In addition, manipulation of pore size and pore volume can be carried out to facilitate fast mass transfer of reactants and products, as Zn^{2+} in $ZnCo_2O_4$ can serve as a foaming agent (porogen) to tune the porosity of the $ZnCo_2O_4$-carbon composites during the pyrolysis process [33]. This will directly impact the mass/charge transfer dynamics, the formation of three-phase interface and/or accessibility of the catalytic active sites in the composites.

Nevertheless, one challenge remains in the application of carbon-based nanocomposites

in MFC, which is the formation of biofilms on the cathode surface resulting from the high biocompatibility of carbon nanomaterials [34, 35]. The biofilms will form a physical barrier against mass transfer of ions and oxygen, resulting in an increase of concentration overpotential. For instance, it has been reported that the pH near the surface of the catalyst layer can reach up to 11.6 ± 0.3 in the presence of a biofilm with an external load of 100 Ω, which is significantly higher than that (9.4 ± 0.3) without a biofilm [35]. Based on the Nernst equation, the OH^- accumulation caused by the biofilm would lead to a voltage loss of over 120 mV, which was more than 10 % of the theoretical voltage (ca. 1.1 V). Significantly, ZnO has been found to exhibit an apparent antibacterial property towards both gram-negative and gram-positive bacteria [36]; and the performance can be further enhanced by the formation of nanocomposites with graphene oxide (GO), in particular under photoirradiation that leads to the production of reactive oxygen species, potent bactericidal reagents [37]. This is the primary motivation of the present study, which is focused on the preparation of $ZnCo_2O_4$/carbon nanocomposites that can not only be used as an effective ORR catalyst but also inhibit the growth of biofilms on the MFC cathode surface.

Herein, GO-Zn/Co nanocomposite were prepared by a two-step thermal procedure, hydrothermal treatment of GO and zinc and cobalt acetates followed by controlled pyrolysis at elevated temperatures. The nanocomposites exhibited apparent ORR activity in alkaline media, where Co species served as the ORR active sites. Meanwhile, Zn^{2+} was used as a foaming agent (porogen) to tune the porosity of the GO-Zn/Co nanocomposites, a critical factor that impacted OH^- transport and local pH in the catalyst layer. Furthermore, the antibacterial activity of the ZnO nanoparticles and GO sheets led to effective inhibition of the formation of biofilms on the electrode surface and hence durable cathode performance. Collectively, this led to a remarkable performance in a proof-of-concept MFC where the power output even surpassed that with commercial Pt/C.

2. Experiment section

2.1 Synthesis of graphene oxide

GO was synthesized by using the modified Hummers method [38]. Briefly, 2 g of graphite flakes (99.8%, Alfa Aesar) were mixed with 46 mL of concentrated H_2SO_4 (98%, Fisher Chemicals) and 10 mL of concentrated HNO_3 (65%, Fisher Chemicals) under magnetic stirring for 4 h in an ice bath. 6 g of $KMnO_4$ (99%, Fisher Chemicals) was then slowly added into the mixture at 35 °C for 1 h. The mixture was diluted with 46 mL of Nanopure water (purified by a Barnstead Nanopure water system, resistivity 18.3 MΩ cm) and magnetically stirred for 2 h at 95 °C. When the solution was cooled down to room temperature, an additional 200 mL of Nanopure water and 10 mL of H_2O_2 (30%, Fisher Chemicals) was added. The precipitate was collected via centrifugation at 4500 rpm and washed with 5% HCl for 5 times, affording GO precipitates that were washed with an ample amount of Nanopure water until the pH value of the rinse reached ca. 7, and then dried in an

oven at 70 °C.

2.2 Synthesis of GO-supported nanocomposites

In a typical reaction, 0.15 g of the GO prepared above was dispersed in 30 mL of Nanopure water and 140 mL of ethanol (Fisher Chemicals), into which was then added a total of 3.9 mmol of $Zn(OAc)_2 \cdot 2H_2O$ (99+%, Matheson Coleman & Bell) and $Co(OAc)_2 \cdot 4H_2O$ (99+%, Matheson Coleman & Bell) (with the Zn:Co mole ratio varied from 1:2 to 1:1 and 2:1), followed by the addition of 30 mL of $NH_3 \cdot H_2O$ (32%, Fisher Chemicals) at room temperature. The reaction was conducted at 80 °C under magnetic stirring at 400 rpm for 20 h, and then the mixture was transferred into a 100 mL autoclave for hydrothermal reaction at 150 °C for 3 h. The obtained product was collected by centrifugation at 4500 rpm and washed with water, and dried in an oven at 80 °C. Finally, the product was pyrolyzed at 800 °C for 2 h under a nitrogen atmosphere, and the resulting samples were denoted as GO-Zn/Co (1:2)-800, GO-Zn/Co (1:1)-800, and GO-Zn/Co (2:1)-800.

Three additional samples at the Zn/Co mole ratio of 1:2 were also prepared by following the same procedure but pyrolyzed at different temperatures (600, 700, and 900 °C). The resulting products were referred to as GO-Zn/Co (1:2)-600, GO-Zn/Co (1:2)-700, and GO-Zn/Co (1:2)-900, respectively. Similarly, a control sample was prepared without the addition of $Zn(OAc)_2 \cdot 2H_2O$, which was denoted as GO-CoO_x-800.

2.3 Characterizations

The morphology of the samples was characterized by transmission electron microscopy measurements (TEM, Philips CM300 at 300 kV). The TEM samples were prepared by dropcasting a dilute dispersion of the samples in ethanol onto a TEM grid and drying in a vacuum oven. The specific surface area of the samples was determined by nitrogen adsorption/desorption at 77.3 K using the Brunauer–Emmett–Teller (BET) method. Pore size distribution was determined with a porosimetry analyzer (Micromeritics, ASAP 2020, USA) based on the Barrett–Joyner–Halenda (BJH) adsorption model. X-ray diffraction (XRD) patterns were acquired with a Rigaku Americas Miniflex Plus powder diffractometer operated at 40 kV and 30 mA. Raman spectra were collected on a LabRAM HR Evolution using an Ar ion laser with an excitation wavelength of 514.5 nm. XPS measurements were conducted using a PHI 5400/XPS instrument equipped with an Al K_α source operated at 350 W and 10^{-9} torr. Thermogravimetric analysis (TGA) was conducted with a PerkinElmer Pyris 1 instrument within the temperature range of 100 to 600 °C at the heating rate of 10 °C min^{-1} in air. Metal elements in the composite samples were also quantitatively assessed by inductively coupled plasma-optical emission spectrometric (ICP-OES) measurements with a PerkinElmer Optima instrument.

2.4 Electrochemistry

Electrochemical tests were carried out with a CHI710 workstation and electrochemical impedance studies were conducted using a Gamry Reference 600 instrument. A Ag/AgCl (3

M KCl) and a graphite rod were used as the reference and counter electrode, respectively, while a rotating (gold) ring–(glassy carbon) disk electrode (RRDE) was used as the working electrode. The Ag/AgCl electrode was calibrated against a reversible hydrogen electrode (RHE) and all potentials in the present study were referenced to this RHE. To prepare catalyst inks, 5 mg of the nanocomposites prepared above was dispersed in 2 mL of a water/ethanol (1:2 v:v) mixture along with 100 μL of a 20 wt.% Nafion solution, and the mixture was sonicated for at least 30 min to achieve good dispersion of the materials. Then 20 μL of the inks was dropcast onto the surface of the glassy carbon electrode and dried at room temperature, corresponding to a catalyst loading of 0.203 mg cm^{-2}. Prior to use, the RRDE was polished with 50 nm Al_2O_3 powder and washed with Nanopure water.

To obtain power and polarization curves, linear sweep voltammograms (LSVs) were collected within the potential range of open circuit voltage (OCV) to 50 mV at a potential scan rate of 0.2 mV s^{-1} [15]. In the measurements, the cathode was the working electrode, and the anode was connected to the counter and reference electrodes.

2.5 Antibacterial tests and biomass quantification

Antibacterial tests were carried out using *S. oneidensis* grown in Tryptic Soy Broth (TSB). *S. oneidensis* was first incubated at 30 °C for 24 h and then a single colony was selected to inoculate 3 mL of liquid TSB, under shaking at 30 °C for another 24 h, at the GO-Zn/Co (1:1)-800 concentration of 0, 0.1 and 0.3 mg mL^{-1}. A 96-well plate was used to quantify the bacterial growth with each well filled to a final volume of 200 μL using the as-prepared bacterial solutions at the dilutions (v/v) of 1/2, 1/4, 1/8 and 1/10. After inoculation, bacteria in the 96-well plate were grown at 30 °C for 24 h. Finally, the number of colony forming units (CFU) was counted by visual inspection to quantify the survival cell percentage.

Biomass on the cathode surface was evaluated by the phospholipid method [39]. The biofilm-covered cathodes were taken from the MFC and cut into small pieces with a certain surface area. The samples were prepared by using a procedure described previously [40]. The absorbance of the samples was evaluated by using a Leng Guang 756mc spectrophotometer at 610 nm. The phosphate concentrations were calculated using the regression line from a standard curve, which was obtained by digesting 10, 20, 40, 60, 80 and 150 μL of a 1 mM glycerol-phosphate solution. Finally, the biomass concentration was calculated using the conversion factor of 191.7 μg of biomass C per 100 mmol of phospholipid [39]. All measured biomass was normalized to the surface area of the cathode pieces.

2.6 Assembly and set-up of MFC

Air cathodes were prepared by coating a catalyst layer onto a teflonized carbon cloth (WOS 1002 PHYCHEMi Co. Ltd., China) at a catalyst loading rate of 1 mg cm^{-1} for GO-Zn/Co (1:1)-800 and 0.5 mg cm^{-1} 20 wt.% Pt/C. In detail, the carbon cloth was teflonized by brushing four layers of polytetrafluoroethylene (60 wt.% solution, Sigma Aldrich) on one

side and heat-treated at 370 °C for 20 min. The prepared catalyst ink was then dropcast onto the other side of the teflonized carbon cloth and dried at 80 °C for 1 h. Carbon cloth was directly used as anode after washing in acetone. The prepared anode and air cathode were mounted on the two side of the cubic MFC with a cylindrical chamber of 28 mL in volume. The electrode spacing was 4 cm and the reference-cathode spacing was 1 cm.

The MFC was inoculated with anaerobic digester sludge containing exoelectrogenic bacteria. During the inoculation process, an external resistor of 1000 Ω was connected to the MFC. The MFC was operated under the fed-batch mode at room temperature (30 ± 1 °C). Electrolyte was replenished with a fresh medium when the cell voltage diminished below 50 mV. The growth medium contained acetate (2.4 g L^{-1}), phosphate buffer (50 mM) and trace elements. The power density (P, mW cm^{-2}) was calculated according to $P = VI/A_{cathode}$, where V is the cell voltage, I is the current and $A_{cathode}$ (cm^2) is the projected area of the air cathode (7 cm^2).

3. Results and discussion

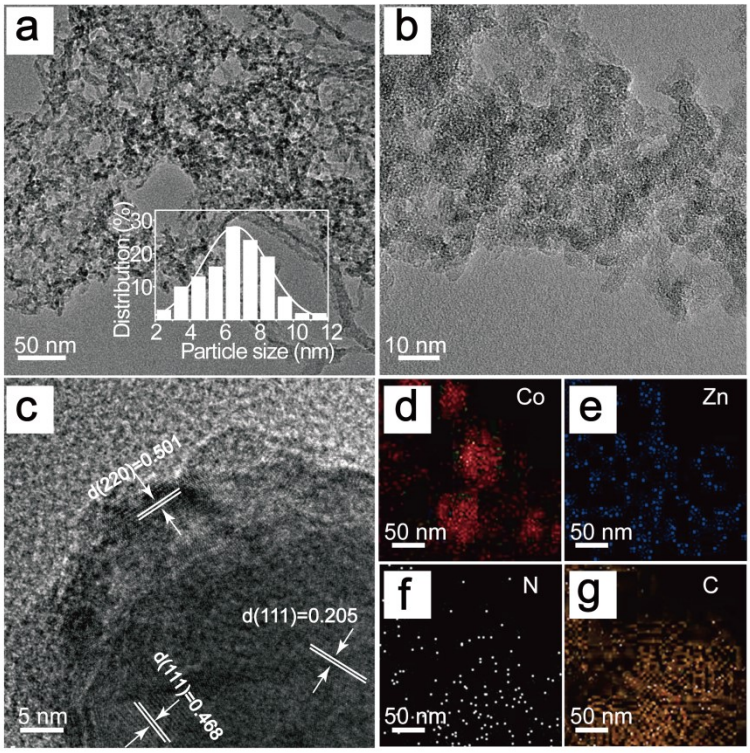

Fig. 1 (a-c) Representative TEM images and (d-g) elemental maps of GO-Zn/Co (1:1)-800. Inset to panel (a) is the particle size histogram.

The GO-Zn/Co nanocomposites were synthesized by a one-pot hydrothermal method where $ZnCo_2O_4$ particles were anchored on GO surfaces, followed by pyrolysis at elevated temperatures. From the TEM images in Fig. 1a-b, one can see that a high density of nanoparticles was distributed on the GO surface. The nanoparticle diameters are mostly within the small range of 6 to 8 nm (Fig. 1a inset), based on the statistical analysis of ca. 120 particles. From high-resolution TEM measurements in Fig. 1c, the nanocomposites can be

seen to exhibit well-defined lattice fringes, where three interplanar distances can be identified at 0.501 nm, 0.205 nm and 0.468 nm. These can be assigned to the (220) planes of graphitic carbon, the (111) planes of metallic Co and the (111) planes of $ZnCo_2O_4$, respectively (Fig. 1c), suggesting the formation of metallic Co and $ZnCo_2O_4$ nanoparticles in the composites [41, 42]. Elemental mapping analysis based on energy dispersive X-ray spectroscopy (EDS) indeed shows the rather homogeneous distributions of Co, Zn, N, and C in the nanocomposite (Fig. 1d-g).

TGA measurements showed that a mass loss of about 5% in air occurred between 350 and 400 °C (Fig. S1), which can be ascribed to (partial) carbon removal from the samples, suggesting that metal oxides were the dominant components in the nanocomposites. In XRD measurements (Fig. S2), the ZnO content was found to diminish appreciably with the pyrolysis temperature increased from 600 to 900 °C, most likely due to its high thermal volatility [33]. This leads to enhanced porosity and specific surface area of the resulting carbon scaffolds, as evidenced in nitrogen adsorption/desorption studies (Fig. S3); and Raman studies showed that the samples exhibited an increasing degree of graphitization (Fig. S4).

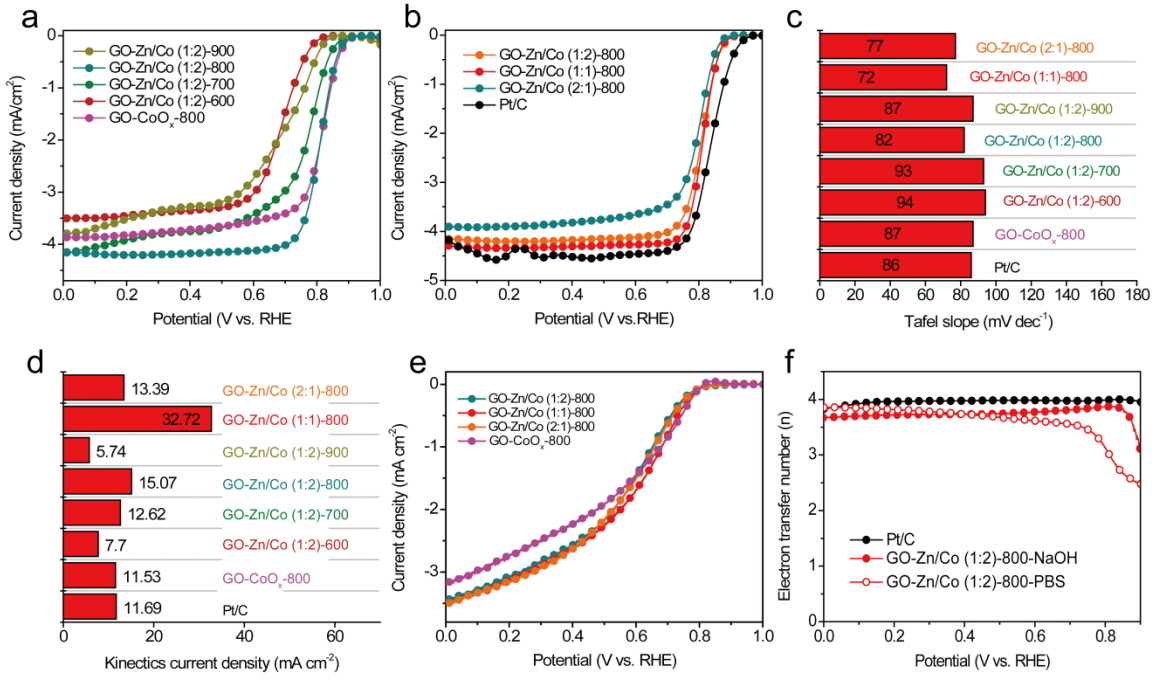

Fig. 2 (a) LSV curves of the series of CO-Zn/Co (1:2) nanocomposites prepared at different temperatures in oxygen-saturated 0.1 M NaOH, (b) LSV curves of the series of CO-Zn/Co nanocomposite catalysts prepared at 800 °C but at different Zn/Co mole ratios in oxygen-saturated 0.1 M NaOH. (c) Tafel slopes and (d) kinetic current density of the nanocomposite catalysts. (e) LSV curves of the nanocomposite catalysts in PBS. (f) Electron transfer numbers of ORR in 0.1 M NaOH and PBS.

Remarkably, the as-prepared nanocomposites exhibited apparent ORR catalytic activity, as manifested in LSV tests (Fig. S5 and S6). Among the series prepared at the Zn/Co mole

ratio of 1:2 but at different pyrolysis temperatures, the GO-Zn/Co (1:2)-800 sample exhibited the most positive onset/halfwave potential at +0.88/+0.81 V vs. RHE and highest limiting current of 4.21 mA cm^{-2} (Fig. 2a), demonstrating that 800 °C was the optimal pyrolysis temperature. The ORR performance was further enhanced by manipulating the Zn/Co mole ratio. From Fig. 2b, it can be seen that GO-Zn/Co (1:2)-800, GO-Zn/Co (1:1)-800 and GO-Zn/Co (2:1)-800 showed the onset/half-wave potentials of +0.88/+0.81, +0.88/+0.81 and +0.86/+0.80 V vs. RHE, and limiting current density of 4.21, 4.34, 3.90 mA cm^{-2}, respectively. This indicates that the GO-Zn/Co (1:1)-800 sample stood out as the best ORR catalysts within the present experimental context, with the most positive onset/half-wave potential and highest limiting current (Fig. 2b). Notably, the half-wave potential of GO-Zn/Co (1:1)-800 was only about 20 mV lower than Pt/C, comparable to the best values reported for cobalt based catalysts (Table S1). This enhancement likely arose from the highest Co-N and pyridinic-N contents in the sample (Table S2 and S3), which are generally regarded as ORR active sites [43-46], in combination with a considerably high degree of graphitization and specific surface area, as determined by XPS, Raman, BET and ICP-OES measurements (Fig. S3, S4 and S7, Table S2-S4).

The Tafel slopes of GO-Co, GO-Zn/Co and Pt/C are then estimated based on the linear region of LSVs at 1600 rpm (at low overpotentials) (Fig. S8a). The results show that the Tafel slope of GO-Zn/Co (1:1)-800 was much lower (72 mV dec^{-1}) than those of Pt/C (86 mV dec^{-1}), GO-CoO_x-800 (87 mV dec^{-1}) and other GO-Zn/Co samples (94, 93, 82 and 87 mV dec^{-1} GO-Zn/Co (1:2)-600, GO-Zn/Co (1:2)-700, GO-Zn/Co (1:2)-800 and GO-Zn/Co (1:2)-900, respectively) (Fig. 2c). Similarly, from the Koutecky-Levich plots (Fig. S8b), the GO-Zn/Co (1:1)-800 sample exhibited the highest kinetic current density (j_K) of 32.72 mA cm^{-2} at +0.6 V among all samples, showing the best ORR kinetics (Fig. 2d). The ORR catalytic performance was also evaluated at neutral pH. The series of GO-Zn/Co catalysts all exhibit a higher limiting current (3.65 mA cm^{-2}) than GO-CoO_x-800 (3.37 mA cm^{-2}) in PBS (pH ~ 7), likely due to improved mass transfer in the GO-Zn/Co catalysts (Fig. 2e). Furthermore, the electron transfer numbers (n) during the ORR process was evaluated by RRDE collection experiments, where the GO-Zn/Co (1:1)-800 sample showed a high n value of ~3.8 and 3.7 in 0.1 M NaOH and PBS at the half-wave potential, similar to that of Pt/C (Fig. 2f).

As the incorporation of Zn into the composites most likely helped improve the catalyst specific surface area and pore volume, and increase the accessibility of catalytic active sites and mass transfer of reactants and products, the electrochemical surface area (ECSA) was then evaluated and compared, as reflected by the electrode double-layer capacitance (C_{dl}). The voltammograms of the catalyst samples are tested at the scan rates of 20 to 100 mV s^{-1} within the potential range of +0.95 to +1.05 V vs. RHE, where no faradaic current was produced (Fig. S9). The C_{dl} was estimated to be 2.02, 2.98, 3.90 and 3.14 mF cm^{-2} for

GO-CoO_x-800, GO-Zn/Co (1:2)-800, GO-Zn/Co (1:1)-800 and GO-Zn/Co (2:1)-800, respectively (Fig. 3a). One can see that Zn indeed effectively increased the C_{dl} of the catalysts, and the GO-Co/Zn (1:1) sample exhibited the highest C_{dl} among the series.

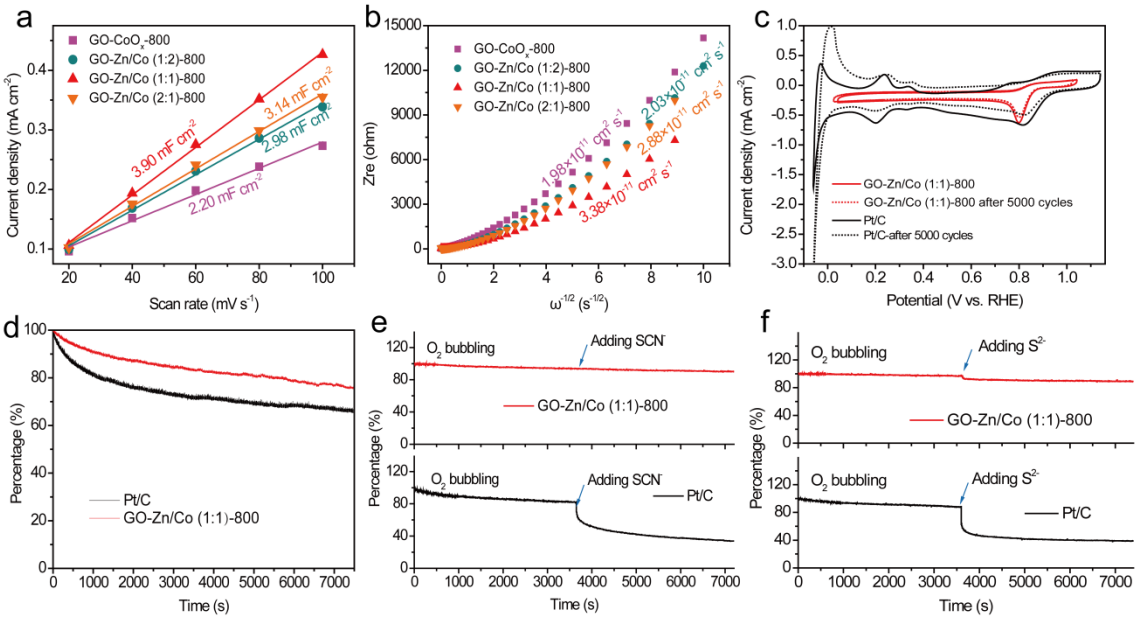

Fig. 3 (a) Double layer capacity of the series of nanocomposite catalysts prepared at different Zn/Co ratios. (b) Variation of Z' with $\omega^{-0.5}$ in the low frequency region. (c) Cyclic voltammograms of GO-Zn/Co (1:1)-800 and Pt/C after 5000 cycles, (d) Chronoamperometric profiles of GO-Zn/Co (1:1)-800 and Pt/C at the potential of +0.7 V vs. RHE. (e) Poisoning tests with the addition of (e) SCN^- (5 mM) and (f) S^{2-} (5 mM) of GO-Zn/Co (1:1)-800 and Pt/C.

Accessibility of catalytic active sites and mass transfer dynamics was then examined by comparing the corresponding diffusion coefficient (D) within the catalyst layer, which can be calculated from the Z' and $\omega^{-0.5}$ plot in the low-frequency region based on equations (1) and (2),

$$Z' = R_s + R_{ct} + \sigma_W \omega^{-0.5} \quad (1)$$

$$D = R^2T^2/(2S^2F^4{\sigma_W}^2C^2) \quad (2)$$

where Z' is the real part of the impedance, ω the angular frequency, and σ_W the slope of Z' against $\omega^{-0.5}$, R, T, S, F, and C are the gas constant, Faraday's constant, absolute temperature, surface area, and molar concentration of electrolyte ions, respectively [1, 47]. From Fig. 3b, the D values of GO-CoO_x-800, GO-Zn/Co (1:2)-800, GO-Zn/Co (1:1)-800 and GO-Zn/Co (2:1)-800 were estimated to be 1.98×10^{-11}, 2.03×10^{-11}, 3.38×10^{-11} and 2.88×10^{-11} $cm^2\ s^{-1}$, respectively. Again, one can see that the GO-Zn/Co (1:1)-800 sample exhibited the highest D value, which coincided with the best ORR activity among the series.

The stability of the as-prepared GO-Zn/Co (1:1)-800 composite was further evaluated by chronoamperometric (CA) and cycle voltammetric (CV) measurements. From Fig. 3c, it can be seen that after 5000 CV cycles, GO-Zn/Co (1:1)-800 showed an obviously slower current

decay than Pt/C. Consistent results were obtained in CA measurements, where ~80% of the current density was retained for GO-Zn/Co (1:1)-800 after 2 h's operation, while only 66% for Pt/C (Fig. 3d). The enhanced stability of GO-Zn/Co (1:1)-800 was probably due to the Co-N and N dopant active sites for ORR.

The GO-Zn/Co (1:1)-800 sample also exhibited markedly enhanced tolerance against chemical poisoning than Pt/C. This is manifested in the CA tests, where the addition of 5 mM SCN^- did not lead to any visible variation of the CA curve for the GO-Zn/Co (1:1)-800 sample, but Pt/C suffered a sharp loss of current (Fig. 3e). In addition, as sulfur-related pollutants are abundant in wastewater which can attack Pt and quickly quench the ORR activity, in the present study, a poison tolerance test with S^{2-} was also carried out with GO-Zn/Co (1:1)-800 and Pt/C. As shown in Fig. 3f, upon the addition of 5 mM S^{2-} into the electrolyte, the ORR current of GO-Zn/Co (1:1)-800 showed only a negligible decrease, whereas Pt/C rapidly diminished by more than 60% of the initial current. These tests demonstrate that the GO-Zn/Co (1:1)-800 sample possessed markedly better poison tolerance and stability than Pt/C in MFC relevant conditions.

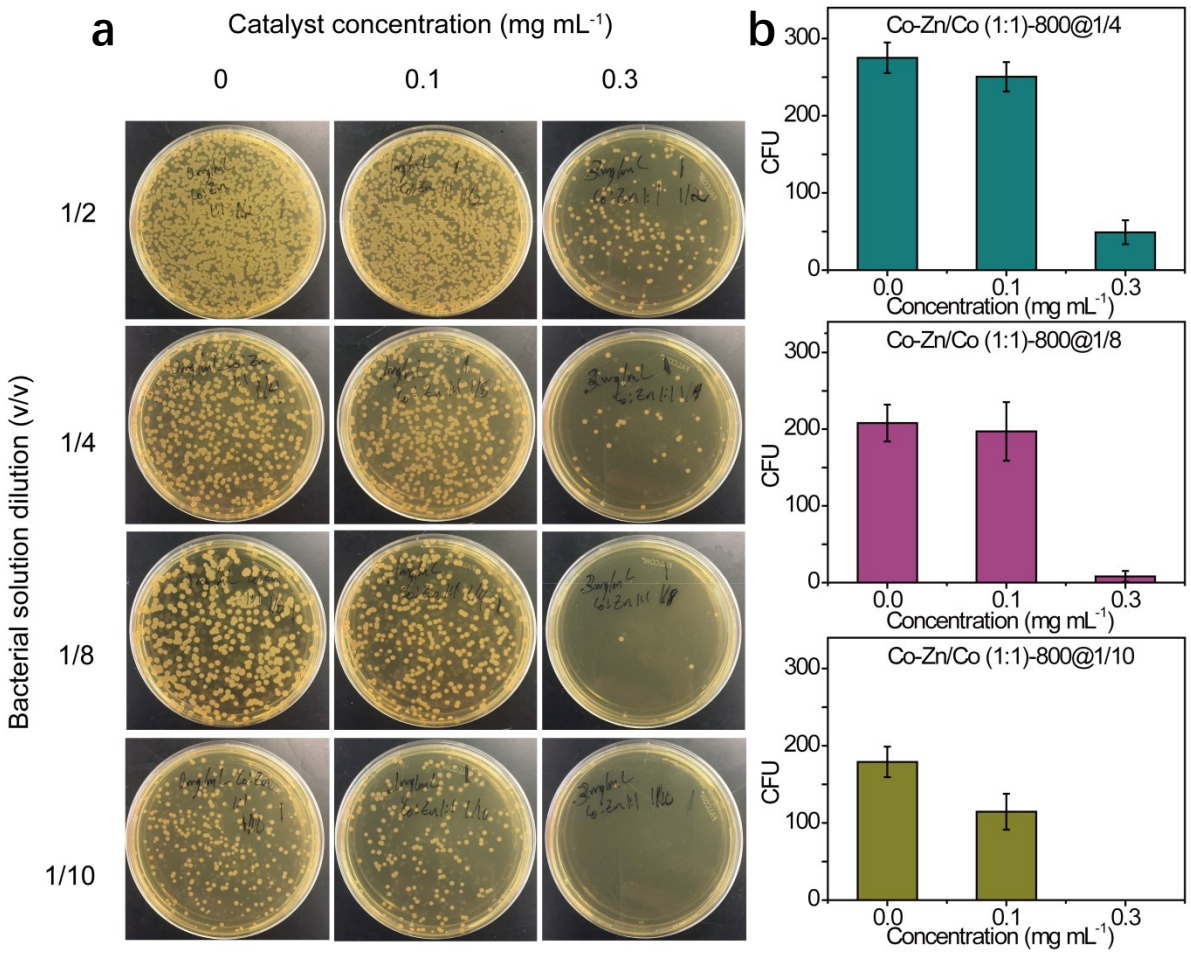

Fig. 4 (a) Photographs and (b) percentage of *S. oneidensis* colonies cultured 24 h in the presence of GO-Zn/Co 1:1-800 at a concentration of 0, 0.1 and 0.3 mg mL^{-1} and a dilution of 1/2, 1/4, 1/8 and 1/10.

As biofilm formation on the cathode surface not only causes OH^- accumulation and increase of concentration overpotential at the electrode, but also leads to deactivation and detachment of the catalyst, it is highly desirable that the catalyst layer also exhibits antibacterial property. The antibacterial activity of the GO-Zn/Co (1:1)-800 was then tested with *S. oneidensis*, which is a commonly used bacterium for substrate degradation and electron generation in MFC. Experimentally, *S. oneidensis* cells were added into the growth media containing 0, 0.1 and 0.3 mg mL^{-1} of GO-Zn/Co (1:1)-800, and the mixture was incubated for 24 h at room temperature before the number of *S. oneidensis* cells was counted. The growth of the bacteria was monitored by counting the number of colony-forming units (CFU), as previously described [36]. Fig. 4a depicts the photographs of *S. oneidensis* colonies culture incubated for 24 h with different catalyst concentrations and different dilution of bacterial solution. It is found that the number of bacterial colonies decreased drastically with the increase of catalyst loading from 0 to 0.3 mg mL^{-1}. More quantitative analysis of the antibacterial activity of GO-Zn/Co (1:1)-800 is illustrated in Fig. 4b. It can be seen that GO-Zn/Co (1:1)-800 exhibited an excellent antibacterial activity. For instance, the number of CFU at the catalyst loading of 0.3 mg mL^{-1} is 49 ± 16, 8 ± 7 and 0 ± 0 at the 1/4, 1/8 and 1/10 dilution, respectively, which is substantially lower than those of the control studies (275 ± 20, 208 ± 24 and 179 ± 20) in which no catalyst was added. These results confirmed that the as-prepared GO-Zn/Co (1:1)-800 catalyst possessed an effective antibacterial activity, holding a potential to inhibit the formation of biofilm in MFC cathodes.

With the high ORR performance, high poison tolerance and stability, and excellent antibacterial property of GO-Zn/Co (1:1)-800, a proof-of-concept MFC was constructed to demonstrate the feasibility of GO-Zn/Co (1:1)-800 as an MFC cathode catalyst, with commercial 20 wt.% Pt/C as the benchmark control. To simulate the real application condition, mixed bacteria from anaerobic digester sludge were used as electrogenic bacteria to degrade the substrate and generate electrons, as previously described [48]. The voltage of the MFC at a 50 Ω external resistance was monitored for 15 d, as shown in Fig. 5a. It can be clearly seen that the voltage output of the MFC using Pt/C cathode significantly decreased from 148 mV to 104 mV over the period of operation, while the decay for the MFC using GO-Zn/Co (1:1)-800 was much slower (from 145 to 125 mV), demonstrating enhanced stability of the GO-Zn/Co (1:1)-800 cathode in practical MFC application. The polarization and power density curves of the as-fabricated MFC using Pt/C and GO-Zn/Co (1:1)-800 are depicted in Fig. 5b. The open circuit voltage for the GO-Zn/Co (1:1)-800 is somewhat lower than that of Pt/C, mainly resulting from the lower open circuit cathode potential. However, the cell voltage of the GO-Zn/Co (1:1)-800 decreased more slowly with the increase of current density, indicating a superior polarization performance and a lower cell internal resistance. Furthermore, the MFC using GO-Zn/Co (1:1)-800 yielded a maximum power density of 773 mW m^{-2}, which is higher than that that with Pt/C (744 mW m^{-2}) under the

same operation condition. Importantly, MFC with GO-Zn/Co (1:1)-800 showed excellent durability and stability after 1 month's continuous operation, with a power density of 566 mW m^{-2}, while MFC using Pt/C cathode decreased to 354 W m^{-2}. The stability of GO-Zn/Co (1:1)-800 was probably due to the antibacterial property that inhibited biofilm formation, and hence alleviated the OH^- accumulation in cathode and the fouling of catalyst. In fact, the biomass on the GO-Zn/Co (1:1)-800 cathode is only 3.62 ± 1.74 mg cm^{-2}, which is significantly lower than that on the Pt/C cathode (11.41 ± 2.05 mg cm^{-2}) (Fig. 5c), signifying much enhanced inhabitation of biofilms in practical applications.

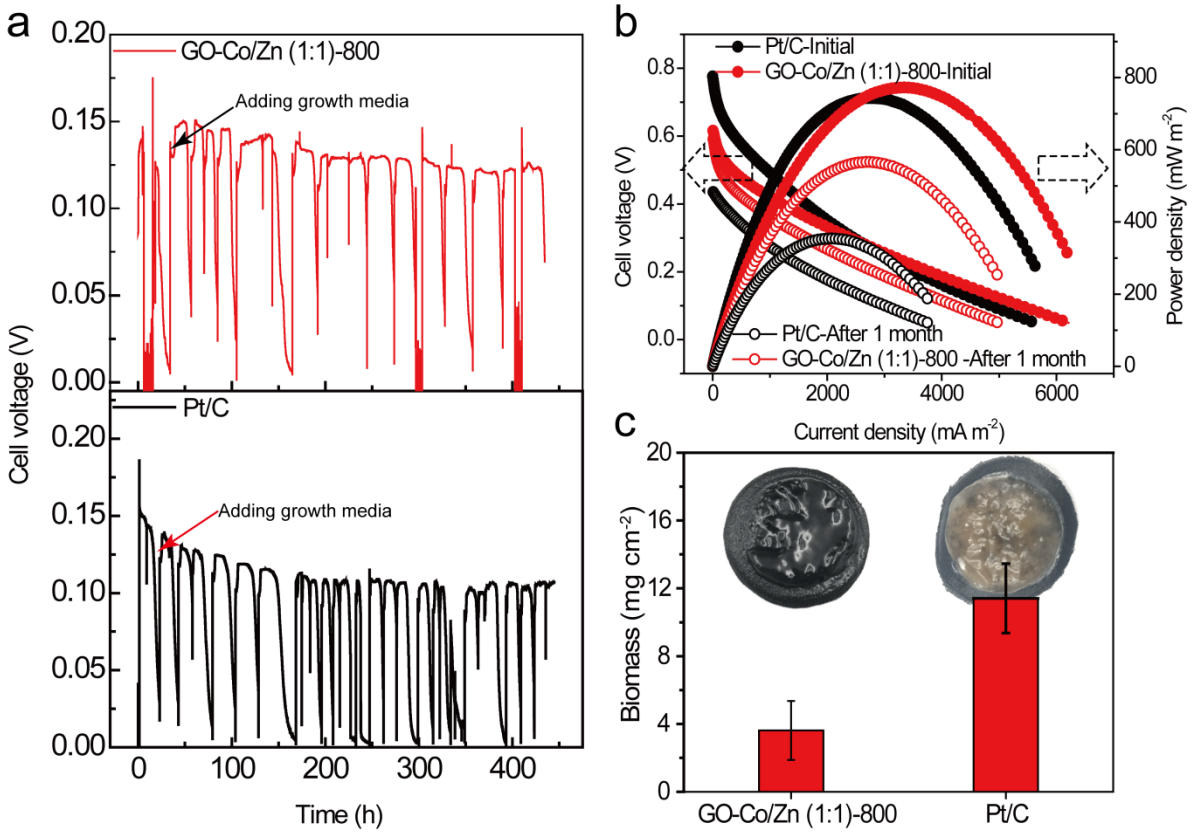

Fig. 5 (a) Cell voltages of MFC using GO-Zn/Co (1:1)-800 and Pt/C catalyst in air cathode, (b) Polarization and power density curves of MFC before and after 1 month's operation, (c) Biomass on the surface of cathodes after 1 month's operation.

4. Conclusion

In this study, GO-Zn/Co nanocomposites based on graphene oxide-supported cobalt and zinc oxide nanoparticles were prepared by pyrolysis at controlled temperatures and varied Zn/Co mole ratio. The sample prepared at 800 °C at the Zn/Co mole ratio of 1:1 was found to exhibit the best ORR activity in alkaline media among the series, most likely due to the combined contributions of a relatively high degree of graphitization, high Co-N concentrations, and high porosity. This was found to lead to enhanced accessibility of the catalytic active centers and mass transfer of reactions and products within the catalyst layer. In comparison to commercial Pt/C, the GO-Zn/Co nanocomposites also exhibited remarkable

tolerance against poisoning pollutants, and inhibition of the formation of biofilms under MFC relevant conditions. These suggest high feasibility of using GO-Zn/Co nanocomposites as MFC cathode catalysts. Indeed, MFC tests showed that the power output was even better than that with Pt/C as the cathode catalyst.

Acknowledgement

Work at CQU was supported by the National Natural Science Funds for Outstanding Young Scholars (No. 51622602), the National Science Foundation for Young Scientists of China (No. 51506017), Scientific Research Foundation for Returned Overseas Chinese Scholars of Chongqing, China (No. cx2017017), Natural Science Foundation of Chongqing, China (No. cstc2017jcyjAX0203), Program for Back-up Talent Development of Chongqing University (No.cqu2018CDHB1A02) and the Fundamental Research Funds for the Central Universities (2018CDXYDL0001). Work at UCSC was supported by the US National Science Foundation (CHE-1710408 and CBET-1848841). W.Y. thanks the China Scholarship Council for a research fellowship.

Competing Interests

The authors declare no competing financial interest

Appendix A. Supplementary Material

Supplementary data associated with this article can be found in the online version at doi:10.1016/

References

[1] S. Zhao, Y. Li, H. Yin, Z. Liu, E. Luan, F. Zhao, Z. Tang, S. Liu, Three-dimensional graphene/Pt nanoparticle composites as freestanding anode for enhancing performance of microbial fuel cells, Sci adv 1 (2015) e1500372.

[2] L. Zhang, J. Li, X. Zhu, D. Ye, Q. Liao, Anodic current distribution in a liter-scale microbial fuel cell with electrode arrays, Chem Eng J, 223 (2013) 623-631.

[3] L. Zhang, X. Zhu, J. Li, Q. Liao, D. Ye, Biofilm formation and electricity generation of a microbial fuel cell started up under different external resistances, J Power Sources, 196 (2011) 6029-6035.

[4] H. Tang, S. Cai, S. Xie, Z. Wang, Y. Tong, M. Pan, X. Lu, Metal–Organic-Framework-Derived Dual Metal-and Nitrogen-Doped Carbon as Efficient and Robust Oxygen Reduction Reaction Catalysts for Microbial Fuel Cells, Adv Sci, 3 (2016) 1500265.

[5] H. Liu, B.E. Logan, Electricity generation using an air-cathode single chamber microbial fuel cell in the presence and absence of a proton exchange membrane, Environmental science & technology, 38 (2004) 4040-4046.

[6] Z. Fu, L. Yan, K. Li, B. Ge, L. Pu, X. Zhang, The performance and mechanism of modified activated carbon air cathode by non-stoichiometric nano Fe 3 O 4 in the microbial fuel cell, Biosens Bioelectron, 74 (2015) 989-995.

[7] B.H. Kim, I.S. Chang, G.M. Gadd, Challenges in microbial fuel cell development and operation, Appl Microbiol Biotechnol, 76 (2007) 485.
[8] F. Zhao, R.C. Slade, J.R. Varcoe, Techniques for the study and development of microbial fuel cells: an electrochemical perspective, Chem Soc Rev, 38 (2009) 1926-1939.
[9] U. Schröder, Anodic electron transfer mechanisms in microbial fuel cells and their energy efficiency, Phys Chem Chem Phys, 9 (2007) 2619-2629.
[10] D. Prasad, S. Arun, M. Murugesan, S. Padmanaban, R. Satyanarayanan, S. Berchmans, V. Yegnaraman, Direct electron transfer with yeast cells and construction of a mediatorless microbial fuel cell, Biosens Bioelectron, 22 (2007) 2604-2610.
[11] C. Santoro, R. Gokhale, B. Mecheri, A. D'Epifanio, S. Licoccia, A. Serov, K. Artyushkova, P. Atanassov, Design of Iron (II) Pthalocyanine (FePc) Derived Oxygen Reduction Electrocatalysts for High Power Density Microbial Fuel Cells, Chemsuschem, (2017).
[12] R.A. Rozendal, H.V. Hamelers, C.J. Buisman, Effects of membrane cation transport on pH and microbial fuel cell performance, Environ Sci Technol, 40 (2006) 5206-5211.
[13] A.Y. Cetinkaya, O.K. Ozdemir, E.O. Koroglu, A. Hasimoglu, B. Ozkaya, The development of catalytic performance by coating Pt–Ni on CMI7000 membrane as a cathode of a microbial fuel cell, Bioresour Technol, 195 (2015) 188-193.
[14] H. Dong, H. Yu, X. Wang, Catalysis kinetics and porous analysis of rolling activated carbon-PTFE air-cathode in microbial fuel cells, Environ Sci Technol, 46 (2012) 13009-13015.
[15] C. Santoro, A. Serov, L. Stariha, M. Kodali, J. Gordon, S. Babanova, O. Bretschger, K. Artyushkova, P. Atanassov, Iron based catalysts from novel low-cost organic precursors for enhanced oxygen reduction reaction in neutral media microbial fuel cells, Energy Environ Sci, 9 (2016) 2346-2353.
[16] S. Khilari, S. Pandit, J.L. Varanasi, D. Das, D. Pradhan, Bifunctional manganese ferrite/polyaniline hybrid as electrode material for enhanced energy recovery in microbial fuel cell, ACS Appl Mater Interfaces, 7 (2015) 20657-20666.
[17] C. Santoro, A. Serov, R. Gokhale, S. Rojas-Carbonell, L. Stariha, J. Gordon, K. Artyushkova, P. Atanassov, A family of Fe-NC oxygen reduction electrocatalysts for microbial fuel cell (MFC) application: Relationships between surface chemistry and performances, Appl Catal B: Environ, 205 (2017) 24-33.
[18] R. Burkitt, T. Whiffen, E.H. Yu, Iron phthalocyanine and MnOx composite catalysts for microbial fuel cell applications, Appl Catal B: Environ, 181 (2016) 279-288.
[19] T. Yang, K. Li, L. Pu, Z. Liu, B. Ge, Y. Pan, Y. Liu, Hollow-spherical Co/NC nanoparticle as an efficient electrocatalyst used in air cathode microbial fuel cell, Biosens Bioelectron, 86 (2016) 129-134.
[20] J. Huang, N. Zhu, T. Yang, T. Zhang, P. Wu, Z. Dang, Nickel oxide and carbon nanotube composite (NiO/CNT) as a novel cathode non-precious metal catalyst in microbial fuel cells, Biosens Bioelectron, 72 (2015) 332-339.
[21] T.W. Kim, M.A. Woo, M. Regis, K.S. Choi, Electrochemical Synthesis of Spinel Type ZnCo2O4 Electrodes for Use as Oxygen Evolution Reaction Catalysts, J Phys Chem Lett, 5 (2014) 2370-2374.
[22] X.-B. Gong, S.-J. You, X.-H. Wang, J.-N. Zhang, Y. Gan, N.-Q. Ren, A novel stainless

steel mesh/cobalt oxide hybrid electrode for efficient catalysis of oxygen reduction in a microbial fuel cell, Biosens Bioelectron, 55 (2014) 237-241.
[23] Z.Q. Liu, H. Cheng, N. Li, T.Y. Ma, Y.Z. Su, ZnCo2O4 Quantum Dots Anchored on Nitrogen-Doped Carbon Nanotubes as Reversible Oxygen Reduction/Evolution Electrocatalysts, Adv Mater, 28 (2016) 3777-3784.
[24] J. Bai, X.G. Li, G.Z. Liu, Y.T. Qian, S.L. Xiong, Unusual Formation of ZnCo2O4 3D Hierarchical Twin Microspheres as a High-Rate and Ultralong-Life Lithium-Ion Battery Anode Material, Adv Funct Mater, 24 (2014) 3012-3020.
[25] T.F. Hung, S.G. Mohamed, C.C. Shen, Y.Q. Tsai, W.S. Chang, R.S. Liu, Mesoporous $ZnCo_2O_4$ nanoflakes with bifunctional electrocatalytic activities toward efficiencies of rechargeable lithium-oxygen batteries in aprotic media, Nanoscale, 5 (2013) 12115-12119.
[26] X.J. Liu, Z. Chang, L. Luo, T.H. Xu, X.D. Lei, J.F. Liu, X.M. Sun, Hierarchical $ZnxCo_{3-x}O_4$ Nanoarrays with High Activity for Electrocatalytic Oxygen Evolution, Chem Mater, 26 (2014) 1889-1895.
[27] Y.P. Huang, Y.E. Miao, H.Y. Lu, T.X. Liu, Hierarchical $ZnCo_2O_4$@$NiCo_2O_4$ Core-Sheath Nanowires: Bifunctionality towards High-Performance Supercapacitors and the Oxygen-Reduction Reaction, Chem-Eur J, 21 (2015) 10100-10108.
[28] D. Bin, B.B. Yang, F.F. Ren, K. Zhang, P. Yang, Y.K. Du, Facile synthesis of PdNi nanowire networks supported on reduced graphene oxide with enhanced catalytic performance for formic acid oxidation, J Mater Chem A, 3 (2015) 14001-14006.
[29] H. Xu, B. Yan, S.M. Li, J. Wang, C.Q. Wang, J. Guo, Y.K. Du, Facile Construction of N-Doped Graphene Supported Hollow PtAg Nanodendrites as Highly Efficient Electrocatalysts toward Formic Acid Oxidation Reaction, ACS Sustain Chem Eng, 6 (2018) 609-617.
[30] D.L. Wang, H.L.L. Xin, R. Hovden, H.S. Wang, Y.C. Yu, D.A. Muller, F.J. DiSalvo, H.D. Abruna, Structurally ordered intermetallic platinum-cobalt core-shell nanoparticles with enhanced activity and stability as oxygen reduction electrocatalysts, Nat Mater, 12 (2013) 81-87.
[31] Y. Hou, Z.H. Wen, S.M. Cui, S.Q. Ci, S. Mao, J.H. Chen, An Advanced Nitrogen-Doped Graphene/Cobalt-Embedded Porous Carbon Polyhedron Hybrid for Efficient Catalysis of Oxygen Reduction and Water Splitting, Adv Funct Mater, 25 (2015) 872-882.
[32] A. Zitolo, N. Ranjbar-Sahraie, T. Mineva, J.K. Li, Q.Y. Jia, S. Stamatin, G.F. Harrington, S.M. Lyth, P. Krtil, S. Mukerjee, E. Fonda, F. Jaouen, Identification of catalytic sites in cobalt-nitrogen-carbon materials for the oxygen reduction reaction, Nat Commun, 8 (2017) 957.
[33] L.G. Li, J.P. Yu, N. Wang, J. Zhao, B. Fan, S.B. Zeng, S.W. Chen, Structural Engineering of Cathode Materials for Lithium-Sulfur Batteries, Encyclopedia of Inorganic and Bioinorganic Chemistry, Wiley, 2018, pp. accepted.
[34] N. Li, Y. Liu, J. An, C. Feng, X. Wang, Bifunctional quaternary ammonium compounds to inhibit biofilm growth and enhance performance for activated carbon air-cathode in microbial fuel cells, J Power Sources, 272 (2014) 895-899.
[35] Y. Yuan, S. Zhou, J. Tang, In situ investigation of cathode and local biofilm microenvironments reveals important roles of OH–and oxygen transport in microbial fuel cells, Environ Sci Technol, 47 (2013) 4911-4917.

[36] J.L. Liu, M.D. Rojas-Andrade, G. Chata, Y. Peng, G. Roseman, J.E. Lu, G.L. Millhauser, C. Saltikov, S.W. Chen, Photo-enhanced antibacterial activity of ZnO/graphene quantum dot nanocomposites, Nanoscale, 10 (2018) 158-166.
[37] M.D. Rojas-Andrade, G. Chata, D. Rouholiman, J.L. Liu, C. Saltikov, S.W. Chen, Antibacterial mechanisms of graphene-based composite nanomaterials, Nanoscale, 9 (2017) 994-1006.
[38] S. Gilje, S. Han, M. Wang, K.L. Wang, R.B. Kaner, A chemical route to graphene for device applications, Nano Lett, 7 (2007) 3394-3398.
[39] R.H. Findlay, G.M. King, L. Watling, Efficacy of phospholipid analysis in determining microbial biomass in sediments, Appl Environ Microbiol, 55 (1989) 2888-2893.
[40] P. Aelterman, S. Freguia, J. Keller, W. Verstraete, K. Rabaey, The anode potential regulates bacterial activity in microbial fuel cells, Appl Microbiol Biotechnol, 78 (2008) 409-418.
[41] B.K. Guan, D. Guo, L.L. Hu, G.H. Zhang, T. Fu, W.J. Ren, J.D. Li, Q.H. Li, Facile synthesis of ZnCo2O4 nanowire cluster arrays on Ni foam for high-performance asymmetric supercapacitors, J Mater Chem A, 2 (2014) 16116-16123.
[42] M. Kuang, Q.H. Wang, P. Han, G.F. Zheng, Cu, Co-Embedded N-Enriched Mesoporous Carbon for Efficient Oxygen Reduction and Hydrogen Evolution Reactions, Adv Energy Mater, 7 (2017) 1700193.
[43] G. Xu, G.C. Xu, J.J. Ban, L. Zhang, H. Lin, C.L. Qi, Z.P. Sun, D.Z. Jia, Cobalt and cobalt oxides N-codoped porous carbon derived from metal-organic framework as bifunctional catalyst for oxygen reduction and oxygen evolution reactions, J Colloid Interf Sci, 521 (2018) 141-149.
[44] M. Sun, H.J. Liu, Y. Liu, J.H. Qu, J.H. Li, Graphene-based transition metal oxide nanocomposites for the oxygen reduction reaction, Nanoscale, 7 (2015) 1250-1269.
[45] Y.J. Zhang, L.H. Lu, S. Zhang, Z.Z. Lv, D.T. Yang, J.H. Liu, Y. Chen, X.C. Tian, H.Y. Jin, W.G. Song, Biomass chitosan derived cobalt/nitrogen doped carbon nanotubes for the electrocatalytic oxygen reduction reaction, J Mater Chem A, 6 (2018) 5740-5745.
[46] D.W. Liu, R. Qiang, Y.C. Du, Y. Wang, C.H. Tian, X.J. Han, Prussian blue analogues derived magnetic FeCo alloy/carbon composites with tunable chemical composition and enhanced microwave absorption, J Colloid Interf Sci, 514 (2018) 10-20.
[47] R. Wang, M. Yan, H. Li, L. Zhang, B. Peng, J. Sun, D. Liu, S. Liu, FeS2 Nanoparticles Decorated Graphene as Microbial-Fuel-Cell Anode Achieving High Power Density, Adv Mater, (2018) 1800618.
[48] Y. Yang, T. Liu, Q. Liao, D. Ye, X. Zhu, J. Li, P. Zhang, Y. Peng, S. Chen, Y. Li, A three-dimensional nitrogen-doped graphene aerogel-activated carbon composite catalyst that enables low-cost microfluidic microbial fuel cells with superior performance, J Mater Chem A, 4 (2016) 15913-15919.

Gustavo Chata received his B.S. degree in bioengineering from the University of California Merced and is pursuing a Ph.D. degree in Chemistry in the University of California at Santa Cruz (UCSC) under the supervision of Prof. Shaowei Chen. His research interest is primarily focused on rational design of functional nanomaterials for antimicrobial applications.

Yi Peng received his B.S. degree in chemistry in 2014 from Beihang University, Beijing, China, and then went on to UCSC to pursue a Ph.D. degree in chemistry under the supervisor of Prof. Shaowei Chen. His research interests include metal/semiconductor nanoparticle surface functionalization, nanoparticle charge-transfer dynamics, and (single atom) catalysts for electrochemical energy conversion and storage.

Jia Lu received her B.S. degree in Forensic Science in 2011 from San Jose State University. She is currently pursuing a Ph.D. degree in chemistry under the supervision of Prof. Shaowei Chen at UCSC. Her research focuses on the self-assembly and chiroptical response of amphiphilic Janus Nanoparticles for chiral molecular sensing.

Nan Wang received his Bachelor's degree in Applied Chemistry from South China University of Technology (SCUT) in 2014. He is currently pursuing a Ph.D. degree under the supervision of Prof. Shaowei Chen and Prof. Ligui Li in the School of Environment and Energy at SCUT. His dissertation research focuses on the design and synthesis of functional nanomaterials for oxygen reduction reaction and

electrochemical water splitting.

Rene Mercado received his B.S. degree from UCSC in 2015 and stayed on to pursue a Ph.D. degree in Chemistry under the supervision of Prof. Shaowei Chen. His research is focused on the design and engineering of carbon-based functional materials for the electrocatalysis of fuel cell reactions.

Shaowei Chen received his B.S. degree in Chemistry from the University of Science and Technology of China in 1991, and his M.S. and Ph.D. degrees from Cornell University in 1993 and 1996, respectively. Following a postdoctoral appointment in the University of North Carolina at Chapel Hill, he joined the faculty in Southern Illinois University Carbondale in 1998. In 2004, he moved to UCSC. He is currently a Professor of Chemistry and the Faculty Director of the UCSC COSMOS program. His research is focused on Janus nanoparticles, nanoparticle charge-transfer dynamics, high-performance electrocatalysts for electrochemical energy technologies, and antimicrobial activity of nanomaterials.